

# Exploring Molecular Dynamics of Adsorbed CO<sub>2</sub> Species in Amine-Modified Porous Silica by Solid-State NMR Relaxation

Rita Fonseca, Ricardo Vieira, Mariana Sardo, Ildefonso Marin-Montesinos,\* and Luís Mafra\*



Cite This: *J. Phys. Chem. C* 2022, 126, 12582–12591



Read Online

ACCESS |



Metrics & More

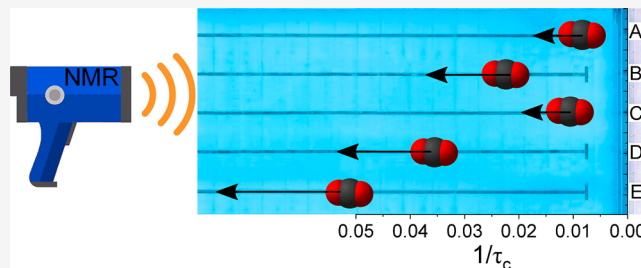


Article Recommendations



Supporting Information

**ABSTRACT:** Previous studies on CO<sub>2</sub> adsorbents have mainly addressed the identification and quantification of adsorbed CO<sub>2</sub> species in amine-modified porous materials. Investigation of molecular motion of CO<sub>2</sub> species in confinement has not been explored in depth yet. This work entails a comprehensive study of molecular dynamics of the different CO<sub>2</sub> species chemi- and physisorbed at amine-modified silica materials through the determination of the rotating frame spin–lattice relaxation times ( $T_{1\rho}$ ) by solid-state NMR. Rotational correlation times ( $\tau_C$ ) were also estimated using spin relaxation models based on the Bloch, Wangsness, and Redfield and the Bloembergen–Purcell–Pound theories. As expected, the  $\tau_C$  values for the two physisorbed CO<sub>2</sub> species are considerably shorter (32 and 20  $\mu$ s) than for the three identified chemisorbed CO<sub>2</sub> species (162, 62, and 123  $\mu$ s). The differences in molecular dynamics between the different chemisorbed species correlate well with the structures previously proposed. In the case of the physisorbed CO<sub>2</sub> species, the  $\tau_C$  values of the CO<sub>2</sub> species displaying faster molecular dynamics falls in the range of viscous liquids, whereas the species presenting slower dynamics exhibit  $T_{1\rho}$  and  $\tau_C$  values compatible with a CO<sub>2</sub> layer of weakly interacting molecules with the silica surface. The values for chemical shift anisotropy (CSA) and <sup>1</sup>H–<sup>13</sup>C heteronuclear dipolar couplings have also been estimated from  $T_{1\rho}$  measurements, for each adsorbed CO<sub>2</sub> species. The CSA tensor parameters obtained from fitting the relaxation data agree with the experimentally measured CSA values, thus showing that the theories are well suited to study CO<sub>2</sub> dynamics in silica surfaces.



## 1. INTRODUCTION

Global warming and associated climate change are a major concern for scientists, politicians, and general public, becoming one of the most important challenges of humankind in the 21st century. Different reports and studies from Intergovernmental Panel on Climate Change, among others, have identified CO<sub>2</sub> emissions to be primary responsible for global warming.<sup>1–3</sup> Among many of the identified sources, flue gas emissions have a major role contributing to the rising of CO<sub>2</sub> levels in the atmosphere.<sup>4,5</sup> Therefore, its scavenging from post-combustion gases combined with other greenhouse gas removal strategies is compulsory to curtail CO<sub>2</sub> emissions.<sup>6,7</sup>

Different materials have been proposed, with amine-modified porous silica (AMPS) sorbents emerging as a promising alternative to the use of liquid amines for CO<sub>2</sub> capture.<sup>8–13</sup> These materials show advantageous features for CO<sub>2</sub> capture in post-combustion applications, such as high selectivity and capture capacity toward CO<sub>2</sub> at low partial pressures even in the presence of moisture. In order to improve the design and optimization of these materials, gathering knowledge on the nature and dynamics of physisorbed and chemisorbed CO<sub>2</sub> species formed is crucial.<sup>14</sup> Several studies have been published in recent years addressing the structure of the different types of CO<sub>2</sub>-amine adducts formed in amine-modified silicas (AMPS),<sup>15–26</sup> mainly performed by Fourier

transform infrared (FT-IR) spectroscopy<sup>15–18</sup> and nuclear magnetic resonance (NMR).<sup>20–30</sup> However, the unambiguous assignment of CO<sub>2</sub> species under certain conditions is still a challenge wherein the tandem use of solid-state NMR and density functional theory (DFT) has provided some of the most prolific results.<sup>21–24</sup> These contributions confirmed the formation of chemisorbed CO<sub>2</sub> species of several types in CO<sub>2</sub>-adsorbed materials containing distinct amine loadings, in which the carbamic acid and alkylammonium carbamate are the predominant CO<sub>2</sub> species. Recently, our group was able to identify, at least, three new physisorbed CO<sub>2</sub> species in SBA-15 mesoporous silica functionalized with a primary amine, 3-aminopropyltriethoxysilane (APTES@SBA-15) combining relaxation and quantitative NMR.<sup>31</sup>

Although the study of CO<sub>2</sub> speciation in AMPS has been reported,<sup>18,20,23,24</sup> information on CO<sub>2</sub> molecular dynamics properties is still scarce. FT-IR or X-ray diffraction methods are

Received: April 18, 2022

Revised: June 24, 2022

Published: July 25, 2022



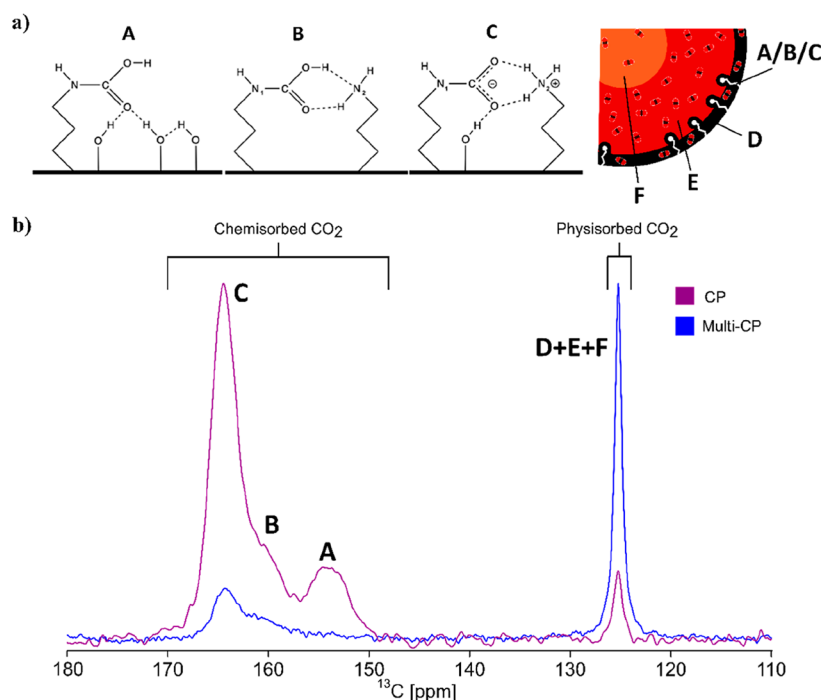


**Figure 1.** (a) Schematic molecular representations correspond to the three different chemisorbed species (A–C) found in APTES@SBA-15 silica loaded with  $^{13}\text{CO}_2$  ( $P = 770$  Torr) as proposed by previous studies.<sup>22,23</sup> The drawing scheme on the right is a simplified picture of a  $\text{CO}_2$ -filled pore of the silica after adsorption, as proposed by our recent work.<sup>31</sup> The different physisorbed species D, E, and F are represented in black, red, and orange colors, respectively. The chemisorbed species are represented by the simplified structures in white. (b)  $^{13}\text{C}$  CPMAS (purple) and MultiCP (blue) NMR spectra of dry APTES@SBA-15 loaded with  $^{13}\text{CO}_2$  at  $p = 770$  Torr. The intensity of the resonance associated to the physisorbed species is low in CPMAS but clearly polarized by MultiCP, contributing to the peak at around 125 ppm.

useful to investigate structural features but have limitations when seeking to understand the molecular dynamics of adsorbates confined in porous systems. Our group has recently investigated  $\text{CO}_2$  dynamics in silicas for the first time by NMR relaxation.<sup>31</sup> Solid-state NMR relaxation techniques have proven to be one of the most valuable approaches, particularly in probing the dynamics of biomolecular systems,<sup>32–37</sup> to observe fluctuations of local environments in adsorbed molecules, often yielding information about local interactions and the motional behavior of molecular moieties.<sup>32,33,38–44</sup> For amorphous materials (like silicas) and non-rigid solids, the correlation times of molecular motions measured by NMR are expected to be in the range of the  $\mu\text{s}$ – $\text{ms}$  timescale.<sup>39</sup> Therefore, the dynamics of adsorbed  $\text{CO}_2$  in AMPS may be investigated by rotating frame spin–lattice relaxation ( $T_{1\rho}$ ) measurements. Recent theoretical developments provide the analytical treatment of  $T_{1\rho}$  as a function of the sample rotation frequency to estimate actual correlation times and amplitudes of motion in solids, particularly in the study of slow protein dynamics.<sup>35,37,45,46</sup>

In this article, we take inspiration on the NMR relaxation studies demonstrated in protein dynamics and perform for the first time  $T_{1\rho}$  measurements to explore the dynamics of physisorbed and chemisorbed  $\text{CO}_2$  species formed at the silica surface, applying the theoretical model proposed by Kurbanov et al.<sup>45</sup> This formalism estimates average  $^{13}\text{C}$ – $^1\text{H}$  distances and  $^{13}\text{C}$  chemical shift anisotropy (CSA) parameters. The study of  $T_{1\rho}$  allows assessing the correlation times for each  $^{13}\text{CO}_2$  species, thus providing a molecular level insight into the dynamics of each  $\text{CO}_2$  species formed in AMPS materials.

## 2. MATERIALS AND METHODS

**2.1. Material Preparation.** SBA-15 was synthesized according to a procedure reported previously by our group.<sup>20</sup> First,  $(\text{EO})_{20}(\text{PO})_{70}(\text{EO})_{20}$  copolymer (4.0 g; Aldrich) was dissolved in a 1.6 M solution of HCl (126  $\text{cm}^3$ ). Next, tetraethyl orthosilicate (9.1  $\text{cm}^3$ ; Aldrich) was added to this solution with constant stirring. The solution was then stirred at 40  $^\circ\text{C}$  for 20 h and subsequently heated at 100  $^\circ\text{C}$  for 24 h, under static conditions. Afterward, the solution was filtered, and the obtained solid was washed with deionized water and dried in an oven at 40  $^\circ\text{C}$ . The solid was calcined at 550  $^\circ\text{C}$  for 5 h with a heating ramp of 1  $^\circ\text{C}/\text{min}$ . The resulting SBA-15 product was stored in a desiccator for further use.

The calcined SBA-15 was functionalized with a primary amine, APTES (Sigma-Aldrich, purity > 98%). 2 g of SBA-15 was introduced in a closed reflux apparatus connected to a vacuum line and heated to 150  $^\circ\text{C}$  for 2 h. After cooling, nitrogen was introduced into the system prior to the opening of the reflux apparatus, and SBA-15 was refluxed with 100  $\text{cm}^3$  of dry toluene (Alfa Aesar, 99.8%) containing 9 mmol of APTES for 24 h in a nitrogen atmosphere. The resulting material (APTES@SBA-15) was purified by Soxhlet extraction with dry toluene, to remove the unreacted amino-alkoxysilane, and finally dried under vacuum, at 120  $^\circ\text{C}$  for 24 h.

**2.2.  $^{13}\text{CO}_2$  Sorption Procedure.** The sorption apparatus comprises a laboratory-made high-vacuum line, connected to a turbomolecular pumping station (HiCube 80, Pfeiffer Vacuum), capable of vacuum greater than  $10^{-2}$  Pa. A borosilicate glass cell was connected to the vacuum line and served as an enclosure for an NMR rotor to allow degassing and heating zirconia NMR rotors up to 300  $^\circ\text{C}$  under high vacuum. The heating was performed with a laboratory-made oven connected

to a power controller (Eurotherm 3116), and the temperature was measured with a thermocouple. The desired gas was introduced into the system from the canister connected to the vacuum line and the cell. The pressure inside the cell was measured with a capacitance transducer (MKS instruments, Baratron 722B).

All samples of APTES@SBA-15 were packed in zirconia NMR rotors, enclosed into the sorption apparatus, and dried by degassing and heating (150 °C, 3 h, ramp of 2.5 °C/min) under vacuum. After cooling down under vacuum,  $^{13}\text{CO}_2$  (Cortecnet, 99 atom %  $^{13}\text{C}$ ; <3 atom %  $^{18}\text{O}$ ) was introduced into the system at a partial pressure of 770 Torr and allowed to equilibrate for 4.5 h. Finally, the NMR rotor was closed inside the cell, and only then, the cell was opened to remove the rotor for NMR measurements.

**2.3. Solid-State NMR Measurements.** All  $^{13}\text{C}$  NMR spectra were acquired on a Bruker Avance III 400 spectrometer operating at  $B_0$  field of 9.4 T, with a  $^{13}\text{C}$  Larmor frequency of 100.6 MHz. All experiments were performed on a double-resonance 4 mm Bruker magic-angle-spinning (MAS) probe at a MAS frequency of 10 kHz and under room temperature conditions. Samples were packed into  $\text{ZrO}_2$  rotors with Kel-F caps.  $^{13}\text{C}$  chemical shifts are quoted in parts per million (ppm) from  $\alpha$ -glycine (secondary reference,  $\text{C}=\text{O}$  at 176.03 ppm).

The  $^{13}\text{C}$  cross-polarization MAS (CPMAS) spectrum, as shown in Figure 1, was acquired under the following experimental conditions: the  $^1\text{H}$   $\pi/2$  pulse length was set to 3.0  $\mu\text{s}$  corresponding to a radio frequency (rf) of  $\sim 83$  kHz; the CP step was performed with a contact time ( $\text{CT}_1$ ) of 3000  $\mu\text{s}$  using a 50–100% RAMP shape pulse in the  $^1\text{H}$  channel and using a 55 kHz square shape pulse on the  $^{13}\text{C}$  channel; the recycling delay ( $D_1$ ) was 7.5 s. During the acquisition, SPINAL-64 decoupling was employed at a rf-field strength of 70 kHz. The total number of scans was 256. The multiple cross polarization (multiCP) sequence, as shown in Figure S1, used a total of  $n = 6$  CP blocks, fulfilling the Hartmann–Hahn condition at the rf field strengths of 55 kHz in the  $^{13}\text{C}$  channel and 48 kHz in the  $^1\text{H}$  channel with a contact time ( $\text{CT}_2$ ) of 15  $\mu\text{s}$ . The  $^1\text{H}$  rf field strength was ramped from 90 to 100%. The  $D_1$  and the inter-CP-blocks delay ( $D_2$ ) were, respectively, 7.5 and 3 s. During the acquisition, SPINAL-64 was applied at a rf-field strength of 80 kHz. The number of scans was 256.

$^{13}\text{C}$   $T_{1\rho}$  times were measured using the NMR experiments, as shown in Figure S1. These two different approaches were used depending on the type of adsorbed  $\text{CO}_2$  species. The conventional method (Figure S1a) was based on CP-MAS<sup>47</sup> for chemisorbed species and a modified version of multiple cross polarization (multiCP,<sup>48</sup> Figure S1b) for the physisorbed fraction. The labels used for the chemisorbed (A–C) and physisorbed (D–F) species are the same as reported in our previous work.<sup>20,22–24,31</sup> Species F was found to exhibit relaxation parameters ( $T_1$ ) compatible with a highly dynamic environment confined in a porous media.<sup>31</sup>

To measure the  $^{13}\text{C}$   $T_{1\rho}$  after generating  $^{13}\text{C}$  magnetization by CPMAS (species A, B, C, and D) or multiCP (species D and E), the  $^{13}\text{C}$  spins were locked in the  $x,y$ -plane of the rotating frame for a variable time ( $\tau$ ) (Table S2) by applying a locking pulse. Under these conditions, the total locked magnetization in the transverse plane ( $M_\tau$ ) decays exponentially with a specific time constant  $T_{1\rho}$  influenced by the modulation of the transverse relaxation Hamiltonian induced by molecular motions. The remaining  $M_\tau$  magnetization after different locking-field  $\tau$  durations is fitted by the equation

$$M_\tau = \sum_{i=1}^n M_{0,i} e^{-\tau/T_{1\rho,i}} \quad (2.1)$$

where  $M_{0,i}$  is the initial locked magnetization in the transverse plane at thermal equilibrium of each  $^{13}\text{CO}_2$  species  $i$ ,  $n$  is the total number of  $^{13}\text{CO}_2$  species, and  $T_{1\rho,i}$  is the spin–lattice relaxation time in the rotating frame of each  $^{13}\text{CO}_2$  species  $i$ . During the application of the locking field,  $^1\text{H}$  decoupling was not applied to avoid interferences on the relaxation mechanism. In our study, to facilitate the analysis, eq 2.1 was linearized as

$$\ln(M_\tau) = \sum_{i=1}^n \ln(M_{0,i}) - \tau/T_{1\rho,i} \quad (2.2)$$

The  $T_{1\rho}$  values (Table S3) were extracted by fitting the linearized eq 2.2 to the experimental data (Figures S4–S9). The estimated fitted errors are below 10%.

The overlapping resonances of the chemisorbed  $^{13}\text{CO}_2$  species centered at 164, 160, and 154 ppm were deconvoluted using software ssNake 1.1,<sup>49</sup> keeping constant the width and position of the peaks within rows of the same pseudo two-dimensional experiments for  $T_{1\rho}$  measurements (Figure S10).

**2.4. Estimation of the Correlation Times of Adsorbed  $^{13}\text{CO}_2$  Species.** To extract the motional correlation times ( $\tau_c$ ) of physisorbed and chemisorbed species,  $T_{1\rho}$  was measured as a function of the rf locking field strength ( $\omega_1$ ). For each measurement, the  $^{13}\text{C}$  rf field strength during spin-lock was carefully calibrated using a nutation experiment in glycine. The values of  $\omega_1$  used for the correlation time study of each adsorbed component were chosen around the condition  $\omega_1 \approx \gamma B_L$ , where  $B_L$  is the local magnetic field amplitude driving the relaxation mechanism in the rotating frame. The main interaction driving the  $T_{1\rho}$  relaxation is CSA since homonuclear and heteronuclear dipolar couplings are negligible for physisorbed  $\text{CO}_2$  species E and F due to their high mobility. Therefore, for E and F species, Bloembergen–Purcell–Pound theory (BPP theory)<sup>50</sup> can be applied. The used  $\omega_1$  frequencies for each  $\text{CO}_2$  species are listed in Table S2.

The dependence of  $R_{1\rho}$  with respect to  $\tau_c$  for the fast components E and F falls within the fast motional regime ( $\tau_c \ll T_2$ ). In this case, the expression for  $R_{1\rho}$  is given by

$$R_{1\rho} = \frac{1}{T_{1\rho}} = \frac{3/4\gamma(\omega_1\delta)^2}{(1 + 4\omega_1^2\tau_c^2)} \quad (2.3)$$

where  $\gamma$  is the gyromagnetic ratio of  $^{13}\text{C}$ ,  $\delta$  is the reduced anisotropy  $\delta = \delta_{zz} - (1/3)(\delta_{xx} + \delta_{yy} + \delta_{zz})$ , and the rest of the parameters are the same as defined above. For species E, the data obtained at different  $\omega_1$  (Table S3) was fitted with eq 2.3 to extract  $\tau_c$ . In the case of species F, weak locking field pulses to measure  $T_{1\rho}$  are needed to assess its fast motional regime, which is currently not possible with our NMR spectrometer.

For the chemisorbed  $\text{CO}_2$  species A, B, C, and D their dynamical behavior falls within the intermediate case ( $\tau_c \approx T_2$ ). Considering the  $^{13}\text{C}$  nuclei of these species are isolated, that is, without covalently bonded protons and that they involve sp/sp<sup>2</sup>-hybridized carbons with considerable CSA contribution, the most suitable model to explain the  $^{13}\text{C}$  relaxation of these species combines CSA and  $^{13}\text{C}$ – $^1\text{H}$  heteronuclear dipolar coupling contributions. The expression used to fit the experimental data is derived from the Bloch,



Wangsness, and Redfield theory (BWR theory)<sup>51,52</sup> accounting for the considerations from Kurbanov et al.,<sup>45</sup> in which the MAS frequency and the rf offset contributions are included. In fact, the MAS dependence of  $R_{1\rho}$  ( $1/T_{1\rho}$ ) was crucial to obtain good fittings of our experimental data, which provide molecular dynamic processes in the range of microseconds to milliseconds.<sup>33,38,47,48</sup>

The  $^{13}\text{C}$  relaxation rate associated to  $\text{CO}_2$  chemisorbed species, considering an off-resonant  $\omega_1$  locking-field and MAS frequency ( $\omega_r$ ), is given by

$$R_{1\rho(\text{off})} = R_{1\rho(\text{off})}^{\text{CSA}} + R_{1\rho(\text{off})}^{\text{IS}} \quad (2.4)$$

Equation 2.4 is the sum of the relaxation rates under CSA and heteronuclear dipolar mechanisms. According to Rovö,<sup>45</sup> the  $R_{1\rho(\text{off})}^{\text{CSA}}$  is given by

$$R_{1\rho(\text{off})}^{\text{CSA}} = \cos^2\theta_\rho R_1^{\text{CSA}} + \sin^2\theta_\rho R_{1\rho(\text{on})}^{\text{CSA}} \quad (2.5)$$

with

$$R_1^{\text{CSA}} = \frac{2}{15}(\delta\omega_1)^2 J(\omega_1) \quad (2.6)$$

and  $R_{1\rho(\text{on})}^{\text{CSA}}$  written as

$$R_{1\rho(\text{on})}^{\text{CSA}} = \frac{(\delta\omega_1)^2}{135} (2J(\omega_1 - 2\omega_r) + 4J(\omega_1 - \omega_r) + 4J(\omega_1 + \omega_r) + 2J(\omega_1 + 2\omega_r) + 9J(\omega_1)) \quad (2.7)$$

$\delta$  is the reduced CSA,  $\omega_C$  is the resonant frequency of the  $^{13}\text{C}$  spin in question, and  $\theta_\rho$  is the off-resonance angle (the angle between the  $B_0$  and  $B_1$  fields).  $J(\omega)$  is the spectral density functions where  $\omega$  can be replaced by different frequency arguments.

Analogous expressions for the heteronuclear dipolar relaxation mechanism can be derived

$$R_{1\rho(\text{off})}^{\text{IS}} = \cos^2\theta_\rho R_1^{\text{IS}} + \sin^2\theta_\rho R_{1\rho(\text{on})}^{\text{IS}} \quad (2.8)$$

with

$$R_1^{\text{IS}} = \frac{b_{\text{IS}}^2}{10} (J(\omega_1 - \omega_s) + 3J(\omega_1) + 6J(\omega_1 + \omega_s)) \quad (2.9)$$

and

$$R_{1\rho(\text{on})}^{\text{IS}} = \frac{b_{\text{IS}}^2}{10} \left( \frac{2}{3}J(\omega_1 - 2\omega_r) + \frac{4}{3}J(\omega_1 - \omega_r) + \frac{4}{3}J(\omega_1 + \omega_r) + \frac{2}{3}J(\omega_1 + 2\omega_r) + J(\omega_1 - \omega_s) + 3J(\omega_1) + 6J(\omega_s) + 6J(\omega_1 + \omega_s) \right) \quad (2.10)$$

where  $b_{\text{IS}}$  is the  $^{13}\text{C}$ - $^1\text{H}$  dipolar coupling constant and  $\omega_{\text{H}}$  is the  $^1\text{H}$  resonant frequency.

Considering the simplest model with a bond vector motion with only one correlation time and an axially symmetric CSA tensor,  $J(\omega)$  both for the dipolar and CSA relaxation mechanisms can be written as

$$J(\omega) = \frac{2}{5} \left( \frac{(1 - S^2)\tau_c}{1 + (\omega\tau_c)^2} \right) \quad (2.11)$$

$S^2$  is the generalized order parameter describing the amplitude of the motion, and it satisfies the condition  $0 \leq$

$S^2 \leq 1$ , where  $S^2 = 0$  and  $S^2 = 1$  represent the fully disordered and completely rigid states, respectively.<sup>32,45</sup> In the present work, considering the amorphous character of the silica as fully disordered, condition  $S^2 = 0$  has been used. We have used these equations to fit the experimental  $T_{1\rho}$  dependence on the  $\omega_1$  spin-lock field. For the case of A, B, and C, the off-resonance (eq 2.4) was used to fit their  $T_{1\rho}$  evolution with  $\omega_{\text{p}}$ , while for species D, data were fitted considering only the on-resonance part. As a result, correlation times and  $b_{\text{IS}}$  and  $\delta$  values are extracted for these four  $^{13}\text{CO}_2$  species.

### 3. RESULTS AND DISCUSSION

**3.1.  $\text{CO}_2$  Speciation after Adsorption in APTES@SBA-15.** Figure 1 shows the  $^{13}\text{C}$  CPMAS (purple) and multiCP (blue) spectra of APTES@SBA-15. Both spectra display four peaks, corresponding to the chemisorbed and physisorbed  $\text{CO}_2$  species, which have been addressed in previous studies.<sup>15,16,20,22–24,29,31,53</sup> Nevertheless, we provide a brief overview of their assignment for the sake of simplicity. The peak at  $\sim 125$  ppm arises from physisorbed  $^{13}\text{CO}_2$  at the silica surface, corresponding to confined  $\text{CO}_2$  in the pore. The full characterization of the three physisorbed  $\text{CO}_2$  species, dubbed D, E, and F, contributing to this resonance (125 ppm) has been performed previously using quantitative CSA and  $T_1$  relaxation analyses.<sup>31</sup> The other three resonances at  $\sim 154$  ppm (species A),  $\sim 160$  ppm (species B), and  $\sim 164$  ppm (species C) are assigned according to our previous studies,<sup>20–24,31</sup> that is, to carbamic acid species (A, B) and ammonium carbamate species (C). In the next sections, we employ  $T_{1\rho}$  to assess correlation times of each  $\text{CO}_2$  species, which are more facile to monitor for an accurate estimation of the dynamics of the adsorbed  $\text{CO}_2$  species.

**3.2.  $T_{1\rho}$  of  $\text{CO}_2$  Species Formed in  $^{13}\text{CO}_2$ -Adsorbed APTES@SBA-15.** The measured  $T_{1\rho}$  values of  $\text{CO}_2$  species A–F are listed in Table 1. The first clear observation is that  $T_{1\rho}$

**Table 1.**  $T_{1\rho}$ ,  $\tau_c$ ,  $^{13}\text{C}$ - $^1\text{H}$  Dipolar Coupling Constant ( $b_{\text{IS}}$ ) and the Reduced CSA ( $\delta$ ) Values at  $\omega_1 = 30$  kHz for each  $\text{CO}_2$  Species Adsorbed in APTES@SBA-15 after Exposure to 770 Torr of  $^{13}\text{CO}_2$

$^{13}\text{CO}_2$ species	$T_{1\rho}/\text{ms}$	$\tau_c/\mu\text{s}$	$b_{\text{IS}}/\text{Hz}$	$\delta/\text{ppm}$
A	4.7(0.10)	162(32)	6949(325)	71.90(12.95)
B	1.1(0.11)	62(2)	15269(258)	74.60(13.43)
C	1.4(0.03)	123(1)	22132(1087)	49.30(8.89)
D	8.1(0.13)	32(4)	3962(169)	57.70(10.38)
E	9.4(0.90)	20(4)		0.20(0.03)
F	44.0(5.00)			

values for physisorbed species D–F are considerably longer than the values for chemisorbed species A–C. This is expected since the mobility of the former species is higher than the latter ones. The motional averaging of relaxation mechanisms (mainly heteronuclear dipolar couplings and CSA) causes long  $T_{1\rho}$  relaxation times for the species D–F. Particularly, long  $T_{1\rho}$  is obtained for species E and F (Table 1), which according to our previous work<sup>31</sup> are confined  $\text{CO}_2$  phases with liquid-like and gas-like  $T_1$  relaxation rates.  $\text{CO}_2$  species D is engaged in H-bonds with the chemisorbed  $\text{CO}_2$  layer formed on the silica surface.<sup>20,23,31</sup> These interactions are sufficient to restrict the mobility of this species opening routes for a more efficient spin relaxation through dipolar and CSA mechanisms.  $\text{CO}_2$  species F undergoes faster dynamics compared to  $\text{CO}_2$

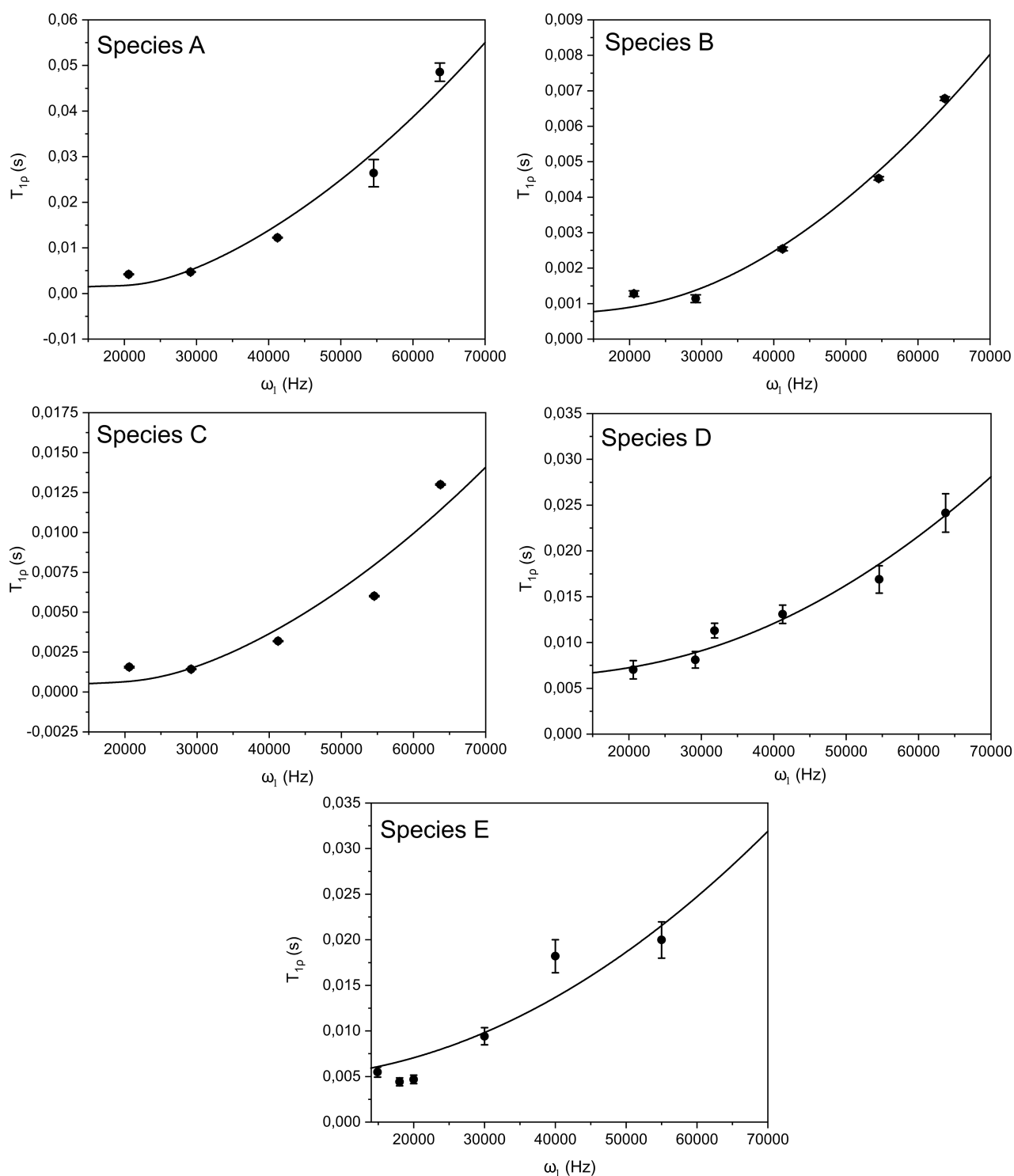


**Figure 2.** Plots of the  $T_{1\rho}$  values for chemisorbed and physisorbed species A, B, C, D, and E as a function of the spin-lock field  $\omega_1$ . The line represents the best fit, using eqs 2.3 and 2.4 for species E and A, B, C, and D, respectively. From this fittings  $\tau_c$ ,  $b_{1S}$  and  $\delta$  values are obtained. The values are presented in Table 1, Figure 3, and Table S3.

species D and E; thus, a much longer  $T_{1\rho}$  value is expected for this species (Table 1).

As for the chemisorbed  $\text{CO}_2$  species A–C, larger  $T_{1\rho}$  differences are found between A and B/C though. These discrepancies can be explained invoking the strength of interactions and the different molecular dynamics. Because species B and C refer to paired amines,<sup>20,22,23</sup> the density of coupled  $^1\text{H}$  spins surrounding these species is higher. The

magnitude of the heteronuclear dipolar couplings of B and C is presumably larger than that in the case of species A, offering a more efficient  $^{13}\text{C}$  relaxation route for B and C.

In addition, A interacts with silanol groups at the silica surface through hydrogen bonds, leading to a strong restriction in motion, which therefore translates in a higher  $\tau_c$  value as it will be discussed ahead.

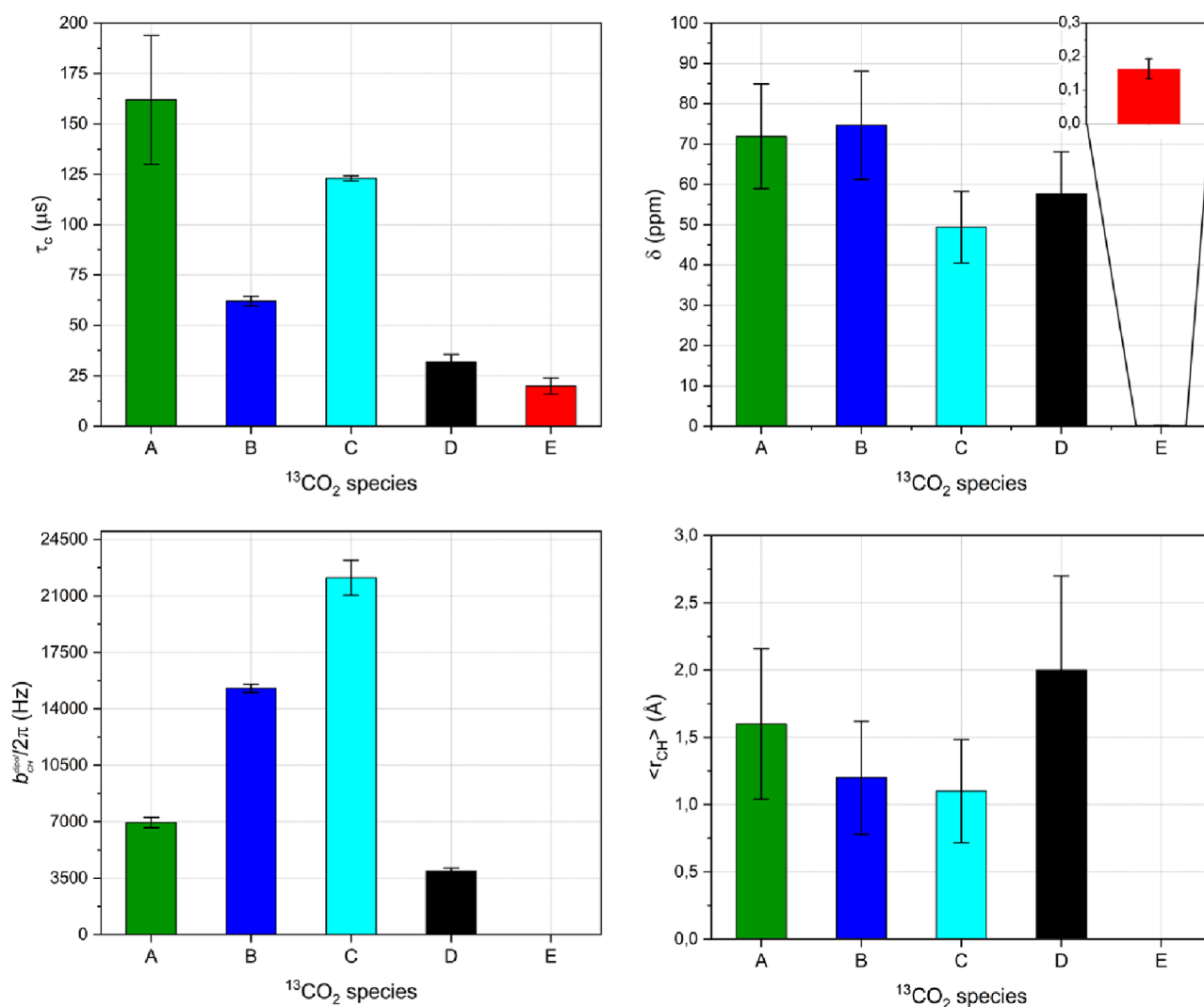


**Figure 3.** Plot bars comparing the different parameters extracted from  $T_{1\rho}$  analysis among the different formed  $^{13}\text{CO}_2$  species. Top left: correlation times ( $\tau_c$ ) showing the different dynamics between species. Top right: reduced CSA ( $\delta$ ). This parameter is related with the degree of confinement, mobility, and interaction with the silica surface of the different species. Bottom left: heteronuclear dipolar coupling constant ( $b_{\text{IS}}$ ) extracted for the different species. The relaxation model used for species E does not consider heteronuclear dipolar coupling as the relaxation mechanism; therefore,  $b_{\text{IS}}$  is absent for E. This parameter provides information about the chemical environment and proximity of chemical groups from the silica surface to the different  $\text{CO}_2$  species. Bottom right: the average distance  $^{13}\text{C}-^1\text{H}$  ( $\langle r_{\text{CH}} \rangle$ ) in Angstroms ( $\text{\AA}$ ) for the adsorbed  $\text{CO}_2$  species. The values are calculated from the fitted  $b_{\text{IS}}$ . The color scheme is as follows: green, blue, cyan, black, and red for the A, B, C, D, and E species, respectively.

**3.3. Correlation Times ( $\tau_c$ ) of the Adsorbed  $\text{CO}_2$  Species in APTES@SBA-15.** Relaxation rates ( $R_{1\rho}$ ) were evaluated by acquiring  $T_{1\rho}$  as a function of the spin-lock field. The resulting curves were fitted (Figure 2) using the relaxation models described in Section 2.4. In the case of the chemisorbed  $\text{CO}_2$  species A, B, and C, the data were fitted using eq 2.4. For the physisorbed  $\text{CO}_2$  species D, the on-resonance part of eq 2.4 was employed, whereas for the physisorbed species E, eq 2.3 was used to fit the data. Detailed parameters obtained from data fittings including estimated correlation times for each  $\text{CO}_2$  species can be found in Table 1 and Figure 3. In the case of  $\text{CO}_2$  species F, the correlation times could not be retrieved due to the difficulties in measuring  $T_{1\rho}$  at different  $\omega_1$  spin-lock field values. Particularly, when the spin-lock field values are several orders of magnitude higher than the size of the interaction driving the relaxation mechanism, or when the locking field is weak, it renders strongly inhomogeneous pulses.

As expected, the shortest  $\tau_c$  is obtained for the physisorbed  $\text{CO}_2$  species D (32  $\mu\text{s}$ ) and E (20  $\mu\text{s}$ ). The obtained values agree with the mobile character of these species as they are weakly interacting inside the pores. However, the obtained  $\tau_c$  values are much longer than the values reported in the literature for  $\text{CO}_2$  in liquid and gas states (typically in the range of picoseconds to nanoseconds).<sup>54–56</sup> These discrepancies in correlation times between bulk and confined  $\text{CO}_2$  reveal the dramatic effect on the dynamics of gases adsorbed in porous materials.<sup>57,58</sup> The  $\tau_c$  value for D is slightly longer than for E, most likely due to the effect of H-bond interactions hindering the motion of  $\text{CO}_2$  species D.

As for chemisorbed species A, B, and C, their  $\tau_c$  values are 2–8 times longer than that for the physisorbed D and E species, thus highlighting the differences in mobility between both fractions. The comparison of the  $\tau_c$  values among the different chemisorbed species reveals striking differences in their molecular dynamics. Species A exhibits the longest  $\tau_c$

(162  $\mu\text{s}$ ), which is in good agreement with rigid structures reported previously,<sup>22,23</sup> where the formation of either carbamic acid species stabilized by H-bonds with neighboring silanol groups or silylpropylcarbamate species are proposed. The formation of both species implies a strong interaction with the silica surface and, therefore, strong molecular rigidity that translates into long correlation times as found in the present work. Species C ( $\tau_c = 123 \mu\text{s}$ ) is more rigid than B ( $\tau_c = 62 \mu\text{s}$ ) since the former might be further stabilized by the formation of H-bond with neighbor silanol groups (Figure 1).

#### 3.4. NMR Interactions Obtained from $R_{1\rho}$ Analysis.

The curve fitting of relaxation rates allows extracting important parameters such as  $b_{\text{IS}}$  and  $\delta$ , which provide further structural information regarding the different  $\text{CO}_2$  species (Table 1). This information is complementary to the determined correlation times further aiding to investigate the  $\text{CO}_2$  structure in confined spaces.

The fitted  $\delta$  values obtained for all the chemisorbed  $\text{CO}_2$  species (A:  $\delta = 71.9$  ppm, B:  $\delta = 74.6$  ppm, and C:  $\delta = 49.3$  ppm) are in good agreement with previously measured values reported elsewhere<sup>27</sup> (A:  $\delta = 78$  ppm, B:  $\delta = 72$  ppm, and C:  $\delta = 52$  ppm). The similarity in the  $\delta$  values for A and B reflects the fact that both possess similar chemical structures (carbamic acid). However, differences in molecular dynamics and structural flexibility exhibited by both species impose different modulation of the CSA relaxation pathways, giving rise to distinct  $\tau_c$  values. For C, the estimated  $\delta$  value is very different compared to both species A and B. This is expected as the  $\text{CO}_2$  species C contains a carbamate ion pair, instead of a carbamic acid moiety.  $\tau_c$  values for species C and A show the same order of magnitude as both species are engaged in additional interactions supposedly with nearby silanol groups from the silica surface.<sup>22,23</sup> In the case of species D, the estimated  $\delta$  was 57.7 ppm, which matches approximately the value measured previously ( $\delta = 57.0$  ppm) by Vieira et al.<sup>31</sup> through  $^{13}\text{C}$  CSA MAS NMR. A  $\delta = 334.5$  ppm has been measured for pure  $\text{CO}_2$  gas at low temperatures (10–20 K), under vacuum ( $2\text{--}4 \times 10^{-6}$  Torr)<sup>59</sup> and has been used by other studies to estimate the  $\tau_c$  of  $\text{CO}_2$  confined in microporous solids.<sup>60</sup> The discrepancy between the  $\delta$  value measured for  $\text{CO}_2$  species D (a gaseous like  $\text{CO}_2$  species judging from the  $\tau_c$  values) in the present work and the previously reported value<sup>60</sup> can be ascribed to different reasons. First, in our work, we are dealing with mesoporous materials instead of microporous. Second, the temperature and pressure conditions in both studies are different. Finally, the importance of the intermolecular interactions established between the  $\text{CO}_2$  molecules with the silica surface in AMPS<sup>31</sup> may have an impact.<sup>31</sup> The estimated  $\delta$  value for the physisorbed  $\text{CO}_2$  species E was 0.2 ppm (Table 1), using eq 2.3 and considering the CSA interaction as the main relaxation source.

In addition to the CSA interaction, the relaxation model for  $\text{CO}_2$  species A–D also involves the  $^1\text{H}\text{--}^{13}\text{C}$  dipolar couplings as an extra relaxation pathway. Due to the proximity of these species to the  $^1\text{H}$  spins belonging to the grafted alkylamine chains,  $^{13}\text{C}$  spins from species A–D are thus strongly coupled with nearby protons. Therefore, the values of the  $^1\text{H}\text{--}^{13}\text{C}$  dipolar couplings for the A–D species with  $^1\text{H}$  in their vicinity were estimated from the  $R_{1\rho}$  curve fittings. For  $\text{CO}_2$  species A, a  $b_{\text{IS}}$  of 6949 Hz was obtained, which corresponds to an average  $^1\text{H}\text{--}^{13}\text{C}$  distance of 1.6 Å (Figure 3). In the case of B and C, the estimated  $b_{\text{IS}}$  values were 15,269 and 22,132 Hz, accounting for an average distance of 1.2 and 1.1 Å,

respectively. These average  $^1\text{H}\text{--}^{13}\text{C}$  distances support the proposed models (Figure 1) for the chemisorbed species A, B, and C. B and C are species involving paired amines; therefore, their proton densities are higher compared to species A, which involves a single amine residue. The estimated  $b_{\text{IS}}$  for species D is 3962 Hz (average  $^1\text{H}\text{--}^{13}\text{C}$  distance of 2.2 Å), a much lower value compared to A, B, and C as this species is far more mobile (i.e., weaker dipolar coupling).

#### 4. CONCLUSIONS

This work demonstrates that relaxation studies based on  $T_{1\rho}$  measurements are a powerful tool to investigate the dynamics of chemi- and physisorbed  $\text{CO}_2$  species formed in AMPS. We observe that the three chemisorbed  $\text{CO}_2$  species (A, B, and C) possessing the highest rigidity give rise to the shortest  $T_{1\rho}$  values (4.7, 1.1, and 1.4 ms); a  $\text{CO}_2$  species with higher flexibility corresponding to the weakly interacting physisorbed  $\text{CO}_2$  species D exhibits an intermediate  $T_{1\rho}$  value (8.1 ms); finally, the highly dynamic physisorbed  $\text{CO}_2$  species E and F possess the longest  $T_{1\rho}$  values (10.0 and 44.0 ms).

Furthermore, the dependence of the  $T_{1\rho}$  with respect to the locking field was also studied allowing to retrieve correlation times ( $\tau_c$ ), which provide further information on the dynamics of  $\text{CO}_2$  confined in AMPS. The variations in  $\tau_c$  values could eventually be correlated to the differences in desorption energy for the different species. We believe the knowledge about the dynamical properties of each  $\text{CO}_2$  species could then be used for the optimization of the regenerability of the sorbent material. The experimental data were fitted using either the BPP theory for the physisorbed  $\text{CO}_2$  species E or the BWR theory for the  $\text{CO}_2$  species A–D. This theoretical analysis also allowed us to extract  $b_{\text{IS}}$  and  $\delta$  values, providing further insights into  $\text{CO}_2$  dynamics and  $\text{CO}_2$  speciation. This analysis was unpractical for  $\text{CO}_2$  species F due to its fast dynamics, which requires weak rf fields beyond the instrumental capability of a typical solid-state NMR spectrometer. The extracted NMR parameters obtained from  $R_{1\rho}$  curve fitting agree well with the ones obtained from previous studies combining solid-state NMR and DFT calculations,<sup>22,23,31</sup> thus consolidating our knowledge concerning the structure of  $\text{CO}_2$  adsorbed in porous materials.

The obtained  $\tau_c$  values corresponding to physisorbed  $\text{CO}_2$  species D and E (32 and 20  $\mu\text{s}$ ) show typical molecular dynamics very close to a viscous liquid (Figure 4), whereas chemisorbed species A, B, and C present a higher rigidity and therefore longer  $\tau_c$  values (162, 62, and 123  $\mu\text{s}$ ), as typically observed in amorphous solids (Figure 4). The dispersion in the  $\tau_c$  values is also higher among chemisorbed than that in physisorbed  $\text{CO}_2$  species. The estimated  $\tau_c$  value for A indicates that this species has the strongest rigidity, owing to its engagement in multiple H-bonds with silanol groups. Furthermore, we show that the  $T_{1\rho}$  relaxation mechanism in the chemisorbed  $\text{CO}_2$  species is mainly driven by a combination of heteronuclear dipolar and CSA interactions. The largest  $b_{\text{IS}}$  values estimated for  $\text{CO}_2$  species B and C suggest they are surrounded by a dense protonated environment. On the other hand, species A possesses a smaller  $b_{\text{IS}}$  (6949 Hz) value compared to both B (15269 Hz) and C (22132 Hz), thus pointing toward the existence of a less protonated environment surrounding those  $\text{CO}_2$  species. The estimated  $b_{\text{IS}}$  value for physisorbed species D (3962 Hz) is also compatible with  $\text{CO}_2$  molecules weakly interacting with the silica surface.



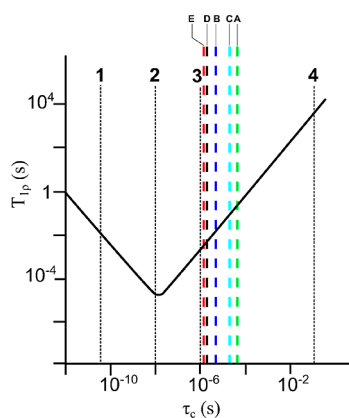


**Figure 4.** Dependence of  $T_{1\rho}$  on  $\tau_c$ , considering the dipole–dipole relaxation mechanism adapted from a study by Farrar et al.<sup>38</sup> Ordinate and abscissa values are only approximate. The dotted lines labeled with numbers represent the correlation times for different matter states: 1 non-viscous liquid, 2 viscous liquid, 3 non-rigid solid, and 4 rigid solid. The dashed lines are the correlation times obtained for species A (green), B (cyan), C (blue), D (black), and E (red).

## ■ ASSOCIATED CONTENT

### SI Supporting Information

The Supporting Information is available free of charge at <https://pubs.acs.org/doi/10.1021/acs.jpcc.2c02656>.

Pulse sequences, pulse durations, and peak integrals of solid-state NMR data for chemi- and physisorbed  $\text{CO}_2$  species (PDF)

## ■ AUTHOR INFORMATION

### Corresponding Authors

**Ildefonso Marin-Montesinos** – CICECO—Aveiro Institute of Materials, Department of Chemistry, University of Aveiro, 3810-193 Aveiro, Portugal; [orcid.org/0000-0002-4206-2643](https://orcid.org/0000-0002-4206-2643); Email: [imarin@ua.pt](mailto:imarin@ua.pt)

**Luís Mafra** – CICECO—Aveiro Institute of Materials, Department of Chemistry, University of Aveiro, 3810-193 Aveiro, Portugal; [orcid.org/0000-0003-1028-8354](https://orcid.org/0000-0003-1028-8354); Email: [lmafra@ua.pt](mailto:lmafra@ua.pt)

### Authors

**Rita Fonseca** – CICECO—Aveiro Institute of Materials, Department of Chemistry, University of Aveiro, 3810-193 Aveiro, Portugal

**Ricardo Vieira** – CICECO—Aveiro Institute of Materials, Department of Chemistry, University of Aveiro, 3810-193 Aveiro, Portugal

**Mariana Sardo** – CICECO—Aveiro Institute of Materials, Department of Chemistry, University of Aveiro, 3810-193 Aveiro, Portugal; [orcid.org/0000-0003-3208-4387](https://orcid.org/0000-0003-3208-4387)

Complete contact information is available at: <https://pubs.acs.org/doi/10.1021/acs.jpcc.2c02656>

### Notes

The authors declare no competing financial interest.

## ■ ACKNOWLEDGMENTS

This work was developed within the scope of the project CICECO-Aveiro Institute of Materials, UIDB/50011/2020 and UIDP/50011/2020, financed by national funds through the Portuguese Foundation for Science and Technology/

MCTES. We also acknowledge funding from the project PTDC/QUI-QFI/28747/2017 (GAS2MAT-DNPSENS - POCI-01-0145-FEDER-028), financed through FCT/MEC and cofinanced by FEDER under the PT2020 Partnership Agreement. The NMR spectrometers are part of the National NMR Network (PTNMR) and are partially supported by Infrastructure Project 022161 (cofinanced by FEDER through COMPETE 2020, POCI, PORL, and FCT through PIDDAC). This work has received funding from the European Research Council (ERC) under the European Union's Horizon 2020 Research and Innovation Program (grant agreement 865974). FCT is also acknowledged by R.V. for a Junior Researcher Position (CEECIND/02127/2017) and by M.S. for an Assistant Research Position (CEECIND/00056/2020).

## ■ REFERENCES

- (1) Intergovernmental Panel on Climate Change. *Climate Change 2014 Synthesis Report*; IPCC, 2014.
- (2) UNFCCC. *Report of the Conference of the Parties on its Twenty-First Session, Held in Paris from 30 November to 13 December 2015*, 2015; p 01194.
- (3) Uk, RSJT. IPCC Special Report 2012. *Global Warming of 1.5°C. An IPCC Special Report on the impacts of global warming of 1.5°C above pre-industrial levels and related global greenhouse gas emission pathways, in the context of strengthening the global response to eradicate poverty*, 2014; pp 659–708.
- (4) Olivier, J. G. J.; Peters, J. A. H. W. *Trends in Global CO<sub>2</sub> and Total Greenhouse Gas Emissions: Report*, 2019.
- (5) IEA (a). *CO<sub>2</sub> Emissions from Fuel Combustion*, 2008.
- (6) Bhattacharyya, D.; Miller, D. C. Post-Combustion CO<sub>2</sub> Capture Technologies — a Review of Processes for Solvent-Based and Sorbent-Based CO<sub>2</sub> Capture. *Curr. Opin. Chem. Eng.* **2017**, *17*, 78–92.
- (7) Modak, A.; Jana, S. Advancement in Porous Adsorbents for Post-Combustion CO<sub>2</sub> Capture. *Microporous Mesoporous Mater.* **2019**, *276*, 107–132.
- (8) Gouedard, C.; Picq, D.; Launay, F.; Carrette, P.-L. Amine Degradation in CO<sub>2</sub> Capture. I. A Review. *Int. J. Greenh. Gas Control* **2012**, *10*, 244–270.
- (9) Zhao, X.; Cui, Q.; Wang, B.; Yan, X.; Singh, S.; Zhang, F.; Gao, X.; Li, Y. Recent Progress of Amine Modified Sorbents for Capturing CO<sub>2</sub> from Flue Gas. *Chin. J. Chem. Eng.* **2018**, *26*, 2292–2302.
- (10) Qin, W.; Egolfopoulos, F. N.; Tsotsis, T. T. Fundamental and Environmental Aspects of Landfill Gas Utilization for Power Generation. *Chem. Eng. J.* **2001**, *82*, 157–172.
- (11) D'Alessandro, D. M.; Smit, B.; Long, J. R. Carbon Dioxide Capture: Prospects for New Materials. *Angew. Chem., Int. Ed.* **2010**, *49*, 6058–6082.
- (12) Wang, J.; Huang, L.; Yang, R.; Zhang, Z.; Wu, J.; Gao, Y.; Wang, Q.; O'Hare, D.; Zhong, Z. Recent Advances in Solid Sorbents for CO<sub>2</sub> Capture and New Development Trends. *Energy Environ. Sci.* **2014**, *7*, 3478–3518.
- (13) Choi, S.; Drese, J. H.; Jones, C. W. Adsorbent Materials for Carbon Dioxide Capture from Large Anthropogenic Point Sources. *ChemSusChem* **2009**, *2*, 796–854.
- (14) Sanz-Pérez, E. S.; Murdock, C. R.; Didas, S. A.; Jones, C. W. Direct Capture of CO<sub>2</sub> from Ambient Air. *Chem. Rev.* **2016**, *116*, 11840–11876.
- (15) Aziz, B.; Hedin, N.; Bacsik, Z. Quantification of Chemisorption and Physisorption of Carbon Dioxide on Porous Silica Modified by Propylamines: Effect of Amine Density. *Microporous Mesoporous Mater.* **2012**, *159*, 42–49.
- (16) Didas, S. A.; Sakwa-Novak, M. A.; Foo, G. S.; Sievers, C.; Jones, C. W. Effect of Amine Surface Coverage on the Co-Adsorption of CO<sub>2</sub> and Water: Spectral Deconvolution of Adsorbed Species. *J. Phys. Chem. Lett.* **2014**, *5*, 4194–4200.



- (17) Bacsik, Z.; Ahlsten, N.; Ziadi, A.; Zhao, G.; Garcia-Bennett, A. E.; Martín-Matute, B.; Hedin, N. Mechanisms and Kinetics for Sorption of CO<sub>2</sub> on Bicontinuous Mesoporous Silica Modified with N-Propylamine. *Langmuir* **2011**, *27*, 11118–11128.
- (18) Yu, J.; Chuang, S. S. C. The Structure of Adsorbed Species on Immobilized Amines in CO<sub>2</sub> Capture: An in Situ IR Study. *Energy Fuels* **2016**, *30*, 7579–7587.
- (19) Zhai, Y.; Chuang, S. S. C. The Nature of Adsorbed Carbon Dioxide on Immobilized Amines during Carbon Dioxide Capture from Air and Simulated Flue Gas. *Energy Technol.* **2017**, *5*, 510–519.
- (20) Mafra, L.; Čendak, T.; Schneider, S.; Wiper, P. v.; Pires, J.; Gomes, J. R. B.; Pinto, M. L. Structure of Chemisorbed CO<sub>2</sub> Species in Amine-Functionalized Mesoporous Silicas Studied by Solid-State NMR and Computer Modeling. *J. Am. Chem. Soc.* **2017**, *139*, 389–408.
- (21) Mafra, L.; Čendak, T.; Schneider, S.; Wiper, P. V.; Pires, J.; Gomes, J. R. B.; Pinto, M. L. Amine Functionalized Porous Silica for CO<sub>2</sub>/CH<sub>4</sub> Separation by Adsorption: Which Amine and Why. *Chem. Eng. J.* **2018**, *336*, 612–621.
- (22) Čendak, T.; Sequeira, L.; Sardo, M.; Valente, A.; Pinto, M. L.; Mafra, L. Detecting Proton Transfer in CO<sub>2</sub> Species Chemisorbed on Amine-Modified Mesoporous Silicas by Using <sup>13</sup>C NMR Chemical Shift Anisotropy and Smart Control of Amine Surface Density. *Chem.—Eur. J.* **2018**, *24*, 10136–10145.
- (23) Afonso, R.; Sardo, M.; Mafra, L.; Gomes, J. R. B. Unravelling the Structure of Chemisorbed CO<sub>2</sub> Species in Mesoporous Aminosilicas: A Critical Survey. *Environ. Sci. Technol.* **2019**, *53*, 2758–2767.
- (24) Sardo, M.; Afonso, R.; Jużków, J.; Pacheco, M.; Bordinhos, M.; Pinto, M. L.; Gomes, J. R. B.; Mafra, L. Unravelling Moisture-Induced CO<sub>2</sub> chemisorption Mechanisms in Amine-Modified Sorbents at the Molecular Scale. *J. Mater. Chem. A* **2021**, *9*, 5542–5555.
- (25) Szego, A. E.; Jaworski, A.; Hedin, N. Chemisorption of CO<sub>2</sub> on Diaminated Silica as Bicarbonates and Different Types of Carbamate Ammonium Ion Pairs. *Mater. Adv.* **2021**, *2*, 448–454.
- (26) Klinkenberg, N.; Kraft, S.; Polzar, S. Great Location: About Effects of Surface Bound Neighboring Groups for Passive and Active Fine-Tuning of CO<sub>2</sub> Adsorption Properties in Model Carbon Capture Materials. *Adv. Mater.* **2021**, *33*, 2007734.
- (27) Heydari-Gorji, A.; Sayari, A. Thermal, Oxidative, and CO<sub>2</sub>-Induced Degradation of Supported Polyethylenimine Adsorbents. *Ind. Eng. Chem. Res.* **2012**, *51*, 6887–6894.
- (28) Lashaki, M. J.; Khiavi, S.; Sayari, A. Stability of Amine-Functionalized CO<sub>2</sub> Adsorbents: A Multifaceted Puzzle. *Chem. Soc. Rev.* **2019**, *48*, 3320–3405.
- (29) Sayari, A.; Belmabkhout, Y.; Da'na, E. CO<sub>2</sub> Deactivation of Supported Amines: Does the Nature of Amine Matter? *Langmuir* **2012**, *28*, 4241–4247.
- (30) Başaran, K.; Topcubasi, B. U.; Davran-Candan, T. Theoretical Investigation of CO<sub>2</sub> adsorption Mechanism over Amine-Functionalized Mesoporous Silica. *J. CO<sub>2</sub> Util.* **2021**, *47*, 101492.
- (31) Vieira, R.; Marin-Montesinos, I.; Pereira, J.; Fonseca, R.; Ilkaeva, M.; Sardo, M.; Mafra, L. hidden” CO<sub>2</sub> in Amine-Modified Porous Silicas Enables Full Quantitative NMR Identification of Physico-Chemisorbed CO<sub>2</sub> Species. *J. Phys. Chem. C* **2021**, *125*, 14797–14806.
- (32) Rovó, P. Recent Advances in Solid-State Relaxation Dispersion Techniques. *Solid State Nucl. Magn. Reson.* **2020**, *108*, 101665.
- (33) Schanda, P.; Ernst, M. Studying Dynamics by Magic-Angle Spinning Solid-State NMR Spectroscopy: Principles and Applications to Biomolecules. *Prog. Nucl. Magn. Reson. Spectrosc.* **2016**, *96*, 1–46.
- (34) Schanda, P.; Kupče, Ě.; Brutscher, B. SOFAST-HMQC Experiments for Recording Two-Dimensional Deteronuclear Correlation Spectra of Proteins within a Few Seconds. *J. Biomol. NMR* **2005**, *33*, 199–211.
- (35) Krushelnitsky, A.; Gauto, D.; Camargo, D. C. R.; Schanda, P.; Saalwächter, K. Microsecond Motions Probed by Near-Rotary-Resonance R 1ρ<sup>15</sup>N MAS NMR Experiments: The Model Case of Protein Overall-Rocking in Crystals. *J. Biomol. NMR* **2018**, *71*, 53–67.
- (36) Marion, D.; Gauto, D. F.; Ayala, I.; Giandoreggio-Barranco, K.; Schanda, P. Microsecond Protein Dynamics from Combined Bloch-McConnell and Near-Rotary-Resonance R 1ρ Relaxation-Dispersion MAS NMR. *ChemPhysChem* **2019**, *20*, 276–284.
- (37) Krushelnitsky, A.; Zinkevich, T.; Reichert, D.; Chevelkov, V.; Reif, B. Microsecond Time Scale Mobility in a Solid Protein as Studied by the 15N R 1ρ Site-Specific NMR Relaxation Rates. *J. Am. Chem. Soc.* **2010**, *132*, 11850–11853.
- (38) Farrar, T. C. Pulsed and Fourier Transform NMR Spectroscopy. *Anal. Chem.* **1970**, *42*, 109–112.
- (39) McBrierty, V. J.; Packer, K. J. *Nuclear Magnetic Resonance in Solid Polymers*; Wiley, 1993.
- (40) Schaefer, J.; Stejskal, E. O.; Buchdahl, R. Magic-Angle C-13 NMR Analysis of Motions in Solid Polymers. *Am. Chem. Soc., Div. Polym. Chem.* **1976**, *17*, 17–22.
- (41) Favre, D. E.; Schaefer, D. J.; Chmelka, B. F. Direct Determination of Motional Correlation Times by 1D MAS and 2D Exchange NMR Techniques. *J. Magn. Reson.* **1998**, *134*, 261–279.
- (42) Strange, J. H.; Mitchell, J.; Webber, J. B. W. Pore Surface Exploration by NMR. *Magn. Reson. Imaging* **2003**, *21*, 221–226.
- (43) Lewandowski, J. R. Advances in Solid-State Relaxation Methodology for Probing Site-Specific Protein Dynamics. *Acc. Chem. Res.* **2013**, *46*, 2018–2027.
- (44) James, T. L.; Matson, G. B.; Kuntz, I. D.; Fisher, R. W.; Buttlare, D. H. Rotating Frame Spin-Lattice Relaxation in the Presence of an off-Resonance Radio Frequency Field. Investigation of Intermediate Molecular Motions. *J. Magn. Reson.* **1977**, *28*, 417–426.
- (45) Kurbanov, R.; Zinkevich, T.; Krushelnitsky, A. The Nuclear Magnetic Resonance Relaxation Data Analysis in Solids: General RIRI Equations and the Model-Free Approach. *J. Chem. Phys.* **2011**, *135*, 184104.
- (46) Krushelnitsky, A.; Zinkevich, T.; Reif, B.; Saalwächter, K. Slow Motions in Microcrystalline Proteins as Observed by MAS-Dependent <sup>15</sup>N Rotating-Frame NMR Relaxation. *J. Magn. Reson.* **2014**, *248*, 8–12.
- (47) Schaefer, J.; Stejskal, E. O.; Buchdahl, R. Magic-Angle <sup>13</sup>C NMR Analysis of Motion in Solid Polycarbonate. *J. Macromol. Sci., Part B: Phys.* **1977**, *13*, 665–672.
- (48) Johnson, R. L.; Schmidt-Rohr, K. Quantitative Solid-State <sup>13</sup>C NMR with Signal Enhancement by Multiple Cross Polarization. *J. Magn. Reson.* **2014**, *239*, 44–49.
- (49) van Meerden, S. G. J.; Franssen, W. M. J.; Kentgens, A. P. M. SsNake: A Cross-Platform Open-Source NMR Data Processing and Fitting Application. *J. Magn. Reson.* **2019**, *301*, 56–66.
- (50) Bloembergen, N.; Purcell, E. M.; Pound, R. Relaxation Effects in Nuclear Magnetic Resonance Absorption. *Phys. Rev.* **1948**, *73*, 679–712.
- (51) Redfield, A. G. On the Theory of Relaxation Processes. *IBM J. Res. Dev.* **2010**, *1*, 19–31.
- (52) Wangsness, R. K.; Bloch, F. The Dynamical Theory of Nuclear Induction. *Phys. Rev.* **1953**, *89*, 728.
- (53) Lee, J. J.; Chen, C.-H.; Shimon, D.; Hayes, S. E.; Sievers, C.; Jones, C. W. Effect of Humidity on the CO<sub>2</sub> Adsorption of Tertiary Amine Grafted SBA-15. *J. Phys. Chem. C* **2017**, *121*, 23480–23487.
- (54) Boeré, R. T.; Kidd, R. G. Rotational Correlation Times in Nuclear Magnetic Relaxation. *Annu. Rep. NMR Spectrosc.* **1983**, *13*, 319–385.
- (55) Holz, M.; Haselmeier, R.; Dyson, A. J.; Huber, H. On the Density Dependence of the Rotational Dynamics of Carbon Dioxide and Its <sup>17</sup>O Quadrupole Coupling Constant. *Phys. Chem. Chem. Phys.* **2000**, *2*, 1717–1720.
- (56) Yasaka, Y.; Kimura, Y. Polarity and Nonpolarity of Ionic Liquids Viewed from the Rotational Dynamics of Carbon Monoxide. *J. Phys. Chem. B* **2015**, *119*, 15493–15501.
- (57) Omi, H.; Ueda, T.; Miyakubo, K.; Eguchi, T. Dynamics of CO<sub>2</sub> Molecules Confined in the Micropores of Solids as Studied by <sup>13</sup>C NMR. *Appl. Surf. Sci.* **2005**, *252*, 660–667.
- (58) Duffy, J. A.; Wilkinson, N. J.; Fretwell, H. M.; Alam, M. A.; Evans, R. Phase Transitions of CO<sub>2</sub> Confined in Nanometer Pores as

Revealed by Positronium Annihilation. *J. Phys. Condens. Matter* **1995**, *7*, L713–L717.

(59) Beeler, A. J.; Orendt, A. M.; Grant, D. M.; Cutts, P. W.; Michl, J.; Zilm, K. W.; Downing, J. W.; Facelli, J. C.; Schindler, M. S.; Kutzelnigg, W. Low-Temperature  $^{13}\text{C}$  Magnetic Resonance in Solids. 3. Linear and Pseudolinear Molecules. *J. Am. Chem. Soc.* **1984**, *106*, 7672–7676.

(60) Inukai, M.; Kurihara, T.; Noda, Y.; Jiang, W.; Takegoshi, K.; Ogiwara, N.; Kitagawa, H.; Nakamura, K. Probing Dynamics of Carbon Dioxide in a Metal-Organic Framework under High Pressure by High-Resolution Solid-State NMR. *Phys. Chem. Chem. Phys.* **2020**, *22*, 14465–14470.

## Recommended by ACS

### NMR Reveals Two Bicarbonate Environments in SBA15-Solid-Amine $\text{CO}_2$ Sorbents

Chia-Hsin Chen, Sophia E. Hayes, *et al.*

JULY 23, 2021  
THE JOURNAL OF PHYSICAL CHEMISTRY C

READ 

### Improved Description of Organic Matter in Shales by Enhanced Solid Fraction Detection with Low-Field $^1\text{H}$ NMR Relaxometry

F. Panattoni, P. C. M. M. Magusin, *et al.*

OCTOBER 21, 2021  
ENERGY & FUELS

READ 

### Minimizing Lineshape Distortions in Static Ultra-wideline Nuclear Magnetic Resonance of Half-Integer Spin Quadrupolar Nuclei

Jonas Koppe and Michael Ryan Hansen

MAY 01, 2020  
THE JOURNAL OF PHYSICAL CHEMISTRY A

READ 

### Evidence of Hydronium Formation in Water–Chabazite Zeolite Using Inelastic Neutron Scattering Experiments and *ab Initio* Molecular Dynamics Simulations

M. Jiménez-Ruiz, F. Rey, *et al.*

FEBRUARY 11, 2020  
THE JOURNAL OF PHYSICAL CHEMISTRY C

READ 

Get More Suggestions >